Heliyon 10 (2024) e27302

Contents lists available at ScienceDirect

Heliyon

journal homepage: www.cell.com/heliyon

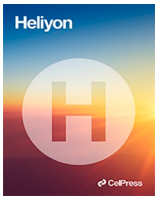

Research article

PANoptosis-related molecule CASP2 affects the immune microenvironment and immunotherapy response of hepatocellular carcinoma

Yichao Lou [1], Desheng Chen [1], Qi Gu, Qi Zhu, Hongcheng Sun [*]

Department of General Surgery, Shanghai General Hospital, Shanghai Jiao Tong University School of Medicine, Shanghai, China

ARTICLE INFO

Keywords:
PANoptosis
CASP2
HCC
Immune
Immunotherapy

ABSTRACT

Background: The involvement of molecules associated with PANoptosis in hepatocellular carcinoma (HCC) is still not well understood.
Methods: Various R packages were utilized to analyze within the R software. Data that was freely accessible was obtained from the databases of The Cancer Genome Atlas (TCGA) and the International Cancer Genome Consortium (ICGC).
Results: Here, we comprehensively explored the role of PANoptosis-related genes in HCC. The caspase 2 (CASP2) was identified as the interest gene for further analysis. We found that CASP2 is related to the poor prognosis and worse clinical features of HCC patients. Moreover, we explored the biological pathway CASP2 is involved in and found that CASP2 is associated with multiple carcinogenic pathways. Also, we noticed that CASP2 can significantly reshape the HCC immune microenvironment and affect the response rate of immunotherapy. Analysis of drug sensitivity suggested that individuals exhibiting elevated CASP2 levels may display increased susceptibility to doxorubicin and vorinostat while demonstrating resistance towards erlotinib, lapatinib, sunitinib, and temsirolimus. Meanwhile, we explored the single-cell distribution of CASP2 in the HCC microenvironment. To enhance the clinical application of CASP2 in HCC, we constructed a prognosis model using the molecules derived from CASP2, which demonstrated good efficiency in predicting patients prognosis. Moreover, in vitro experiments indicated that CASP2 can significantly inhibits cell proliferation, invasion and migration ability of HCC cells.
Conclusions: Our study comprehensively explored the role of PANoptosis-related molecule CASP2 in HCC, which can provide directions for future studies.

1. Introduction

Hepatocellular carcinoma (HCC), the most prevalent form of liver cancer, is ranked fifth worldwide [1,2]. The prognosis for many individuals with HCC is unfavorable because of the restricted ability to detect it early and the limited availability of effective treatments for advanced HCC [3]. Despite the implementation of curative treatments like liver transplantation, resection, percutaneous ablation, and transcatheter arterial chemoembolization, HCC can still experience recurrence and metastasis, resulting in a 5-year survival rate of below 20% [4]. Furthermore, tumor heterogeneity and the presence of both inherent and acquired drug resistance

* Corresponding author.
E-mail address: hongcheng.sun@shgh.cn (H. Sun).
[1] Co-first author.

https://doi.org/10.1016/j.heliyon.2024.e27302
Received 4 December 2023; Received in revised form 27 February 2024; Accepted 27 February 2024
Available online 8 March 2024

can impede the effectiveness of conventional chemotherapy and molecularly targeted medications [5,6]. The effectiveness of systemic treatment in patients with HCC is constrained by these attributes. Hence, it is imperative to investigate novel approaches for enhancing the medical results of individuals with HCC.

PANoptosis is a distinctive, immunoregulatory form of programmed cellular demise, incorporating elements of pyroptosis, apoptosis, and necroptosis [7,8]. It serves as an important regulatory mechanism, orchestrating cell responses to various stimuli, such as inflammation and infection [9]. Recent studies have pinpointed PANoptosis as an essential overseer of immune cell functionality, and any disruption to this process could lead to pathologies, including cancer [10]. Concerning cancer, the function of PANoptosis is intricate and multifactorial [11]. On one end of the spectrum, PANoptosis can function as a deterrent to tumor formation [12]. By facilitating the swift elimination of damaged or aberrant cells, it contributes to tissue homeostasis and acts as a bulwark against the emergence of malignancies [13]. Conversely, the undue activation of PANoptosis within the tumor microenvironment could inadvertently support cancer progression by inducing the demise of immune cells tasked with tumor suppression, thereby aiding immune evasion and inciting inflammation-induced tumorigenesis [14].

Here, we comprehensively explored the role of PANoptosis-related genes in HCC. The caspase 2 (CASP2) was identified as the interest gene for further analysis. We found that CASP2 is related to the poor prognosis and worse clinical features of HCC patients. Moreover, we explored the biological pathway CASP2 is involved in and found that CASP2 is associated with multiple carcinogenic pathways. Also, we noticed that CASP2 can significantly reshape the HCC immune microenvironment and affect the response rate of immunotherapy. Analysis of drug sensitivity suggested that individuals exhibiting elevated CASP2 levels may display increased susceptibility to doxorubicin and vorinostat, while demonstrating resistance towards erlotinib, lapatinib, sunitinib, and temsirolimus. Meanwhile, we explored the single-cell distribution of CASP2 in the HCC microenvironment. To enhance the clinical application of CASP2 in HCC, we constructed a prognosis model using the molecules derived from CASP2, which demonstrated good efficiency in predicting patients prognosis. Moreover, in vitro experiments indicated that CASP2 can significantly inhibit cell proliferation, invasion and migration ability of HCC cells.

2. Methods

2.1. Data acquisition and download

The standardized genomic, and associated clinical data of HCC patients were directly downloaded from The Cancer Genome Atlas (TCGA) and International Cancer Genome Consortium (ICGC) databases [15]. Transcript profile data is downloaded in raw Star-Counts format and eventually converted to TPM format. Clinical data is downloaded in the bcr-xml format and collated using Perl code. For raw transcript profiles, the R code was used for log 2 transformation and gene symbols with mean values less than 0.5 were removed. The list of PANoptosis-related genes was collected from the previous studies [16]. Publicly available cellular subcellular localization data were obtained from the Human Protein Atlas (HPA) database [17]. Sva package was used to combine data from different cohort and remove batch effects [18].

2.2. Pathway enrichment analysis

Significantly enriched pathways were identified based on a corrected p-value below 0.05. The Gene Set Enrichment Analysis (GSEA) was employed to detect gene sets exhibiting notable and consistent disparities between two biological conditions. This analysis involved 1000 permutations of gene sets and a cut-off of <0.25 for the false discovery rate (FDR) q-value [19]. The GSEA analysis utilized reference sets from Gene Ontology (GO), Kyoto Encyclopedia of Genes and Genomes (KEGG), and Hallmark. To display the functionally grouped network of large gene clusters, ClueGO, a plug-in for Cytoscape, was utilized for visualizing the non-duplicate biological terms [20].

2.3. Prognosis analysis

Survival rates were calculated utilizing the Kaplan-Meier (KM) technique, and distinctions among groups were evaluated through the log-rank examination. To determine the factor that significantly impacts patients' survival, both univariate and multivariate logistic regression analyses were performed. The combination of CASP2 and clinical characteristics was used to create a nomogram plot. The calibration plot was employed to assess the agreement between observed and predicted survival using a nomogram. To construct the prognosis model, we initially used univariate Cox regression to assess the correlation between each predictor variable and the outcome of survival.

2.4. Immune microenvironment analysis

The immune microenvironment of the tissue samples was assessed through an array of computational methodologies designed to provide an in-depth understanding of immune cell composition and immune state. To estimate the relative proportions of infiltrating immune cell types, we utilized several deconvolution algorithms, including CIBERSORT, EPIC, MCPCOUNTER, QUANTISEQ, TIMER and XCell [21–26]. Following the quantification of immune cell infiltrates, we utilized single-sample Gene Set Enrichment Analysis (ssGSEA) to quantify the immune status of the tissue [27]. Furthermore, LASSO regression analysis was used to minimize overfitting and perform variable selection. For the variables identified by LASSO regression analysis, multivariate Cox regression was used to

identify the final variables for model construction.

2.5. Immunotherapy and drug sensitivity

The Tumor Immune Dysfunction and Exclusion (TIDE) analysis evaluates the sensitivity of cancer patients to immune checkpoint blockade therapy based on computational modeling of tumor-immune interaction dynamics [28]. The Genomics of Drug Sensitivity in Cancer (GDSC) database is used to assess drug sensitivity, providing a rich resource of large-scale drug response biomarker data, and allowing for the exploration of potential therapeutic targets based on genomic features [29].

2.6. Single-cell analysis

The Tumor Immune Single-cell Hub (TISCH) database serves as a comprehensive resource for the analysis of single-cell data in the context of tumor immunology. It allows researchers to explore, visualize, and compare single-cell RNA sequencing data across a multitude of cancer types, providing detailed insights into the cellular composition and interactions within the tumor microenvironment. This includes the identification of distinct cell types, states, and potential intercellular communication networks [30]. The cohorts with single-cell data obtained from the TISCH project were: GSE98638, GSE125449, GSE140228, GSE166635, GSE146115 and GSE146409 [31–36].

2.7. Cell lines

The THLE-2 human liver cell line, along with liver cancer cell lines HepG2 and Huh7, were acquired from the Shanghai Academy of Chinese Sciences Cell Bank and lab inventory. These cells were cultured in a controlled environment at 37 °C and 5% CO2, with medium replenishment every 2–3 days. The cells were then propagated when approximately 80–90% confluence was achieved.

2.8. Cell transfection

CASP2 small interfering RNAs (siRNAs) were designed and synthesized by Shanghai GenePharma. Cell transfection was executed using Lipofectamine 2000, following the standard procedure. The siRNA sequence is as follows: siRNA#1: 5′-GCACTTCACTGGAGAGAAA-3′, siRNA#2: 5'-GGAGAGTGATGCCGGTAAA-3', siRNA#3, 5′-GGGCTTGTGATATGCACGT-3'.

2.9. Quantitative real-time PCR (qRT-PCR)

RNA was initially extracted using an RNA extraction kit, adhering to the provided protocol. Following this, RNA samples underwent DNase I treatment to eliminate potential gDNA, and total RNA samples were converted into cDNA via reverse transcriptase. Finally, qRT-PCR experiments were carried out using cDNA as a template and adding specific PCR primers (sybr green system). The specific primers used are as follows: CASP2, forward, 5′-AGCTGTTGTTGAGCGAATTGT-3′, reverse, 5′-AGCAAGTTGAGGAGTTCCACA-3'; GAPDH, forward, 5′-GGAGCGAGATCCCTCCAAAAT-3'.

2.10. Cell counting Kit-8 (CCK-8) assay

The cells were seeded onto a 96-well plate at an appropriate density in a culture medium and incubated at 37 °C and 5% CO2 to facilitate cell attachment and recovery. Post-specific treatments, in alignment with experimental needs, the CCK-8 reagent was introduced to each well. The plate was subsequently incubated for 2 h to allow the reaction to occur. Post incubation, absorbance was measured at 450 nm using a microplate reader.

2.11. 5-Ethynyl-2′-deoxyuridine (EdU) assay

Cells were seeded on appropriate plates and incubated under 37 °C and 5% CO2 to facilitate attachment and recuperation. After implementing experimental treatments, EdU (a thymidine analog) was incorporated into the culture medium for a certain duration, usually a few hours, allowing it to be assimilated during active DNA synthesis (S phase of the cell cycle). Post EdU incubation, cells were fixed, typically with paraformaldehyde, to preserve cell morphology and secure the incorporation of EdU. Subsequently, cells underwent permeabilization using an appropriate agent, such as Triton X-100, enabling the entry of detection reagents. DAPI was utilized for nuclear staining. Images were subsequently captured using fluorescence microscopy, and the percentage of EdU-positive cells (cells undergoing DNA synthesis) was determined by counting the number of fluorescent cells relative to the total cell count.

2.12. Transwell assay

Cells were initially prepared in serum-free media and placed onto the upper chamber of a transwell insert (8.0 μm), which was situated in a well of a 24-well plate. The lower chamber of the well was filled with serum-containing media, serving as a chemoattractant. The plate was then incubated under standard conditions for a specific 24-h period, enabling cell migration or invasion through the semi-permeable membrane towards the chemoattractant in the lower chamber. At the end of the incubation period, non-

migrated or non-invaded cells on the upper side of the membrane were eliminated. Cells that migrated or invaded to the underside of the membrane were fixed and stained with crystal violet.

2.13. Statistical analysis

The R software was utilized for all statistical analysis. For the initial data exploration, we utilized descriptive statistics such as the average, and middle value, and measures of variability like standard deviation for continuous variables. Additionally, we examined

A

Gene set	Sensors and Upstream Regulators	Adaptors	Effectors
PANoptosis	AIM2, MEFV, NLRC4, NLRP1, NLRP3, NLRP9, TNFRSF1A, ZBP1	FADD, PYCARD, ACS	CASP1, CASP10, CASP12, CASP2, CASP3, CASP4, CASP5, CASP6, CASP7, CASP8, DFNA5, GSDMD, MLKL, RIPK1, RIPK3, TNF
Pyroptosis	ADAR, AIM2, MEFV, NAIP, NLRC4, NLRP1, NLRP3, NLRP6, NLRP9, ZBP1	PYCARD	CASP1, CASP4, CASP5, CASP8, DFNA5, GSDMA, GSDMB, GSDMC, GSDMD
Necroptosis	ZBP1		CASP8, MLKL. RIPK3
Apoptosis	APAF1, BAX, BAK, DCN, DIABLO,	FADD	CASP2, CASP3, CASP6, CASP7, CASP8, CASP9, CASP10, CASP12, RIPK1, TNF

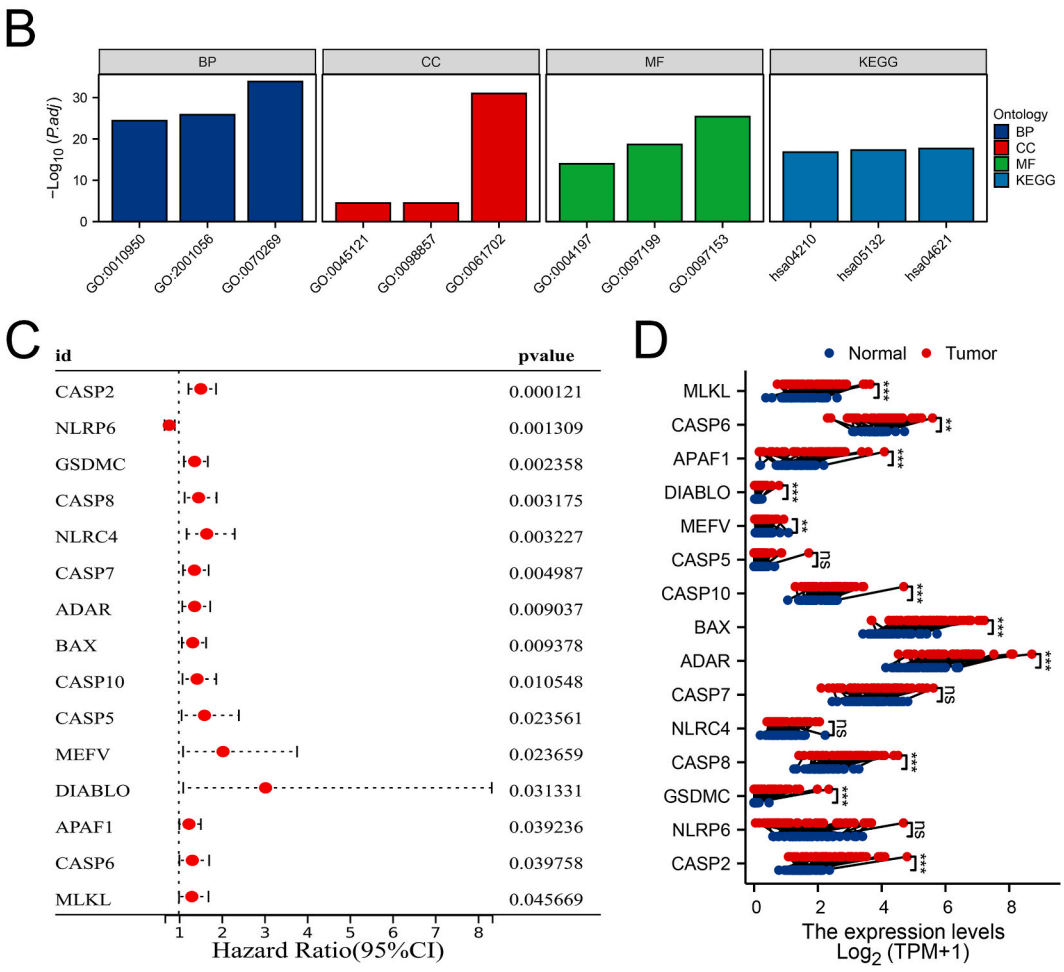

Fig. 1. Identification of PANoptosis-related genes in HCC. **Notes: A:** The PANoptosis-related molecules collected from previous studies; **B:** GO and KEGG analysis of these PANoptosis-related genes; **C:** Univariate Cox regression of these PANoptosis-related genes to identify the molecules significantly associated with patients survival; **D:** The expression level of MLKL, CASP6, APAF1, DIABLO, MEFV, CASP5, CASP10, BAX, ADAR, CASP7, NLRC4, CASP8, GSDMC, NLRP6. CASP2 in tumor and normal tissue.

frequencies and percentages for categorical variables. Comparisons were made using Student's t-tests (or Mann-Whitney U tests for data that is not normally distributed) and chi-square tests (or Fisher's exact tests when applicable). The analysis of differentially expressed genes (DEGs) was performed using the Limma package [37]. The performance of the prognosis model was assessed using Kaplan-Meier (KM) survival and receiver operating characteristic (ROC) curves.

3. Results

3.1. Identification of the PANoptosis-related genes in HCC

The flow chart was shown in Fig. S1. Based on the previous studies, we collected genes involved in the PANoptosis process (Fig. 1A). Then, we performed the GO and KEGG analysis. The results indicated that these PANoptosis-related genes were mainly involved in the regulation of endopeptidase activity (Fig. 1B). Univariate Cox regression analysis indicated that among these molecules, CASP2, NLRP6, GSDMC, CASP8, NLRC4, CASP7, ADAR, BAX, CASP10, CASP5, MEFV, DIABLO, APAF1, CASP6 and MLKL were significantly correlated with patient survival (Fig. 1C). Among them, CASP2 has the most significant P value and is therefore selected for further

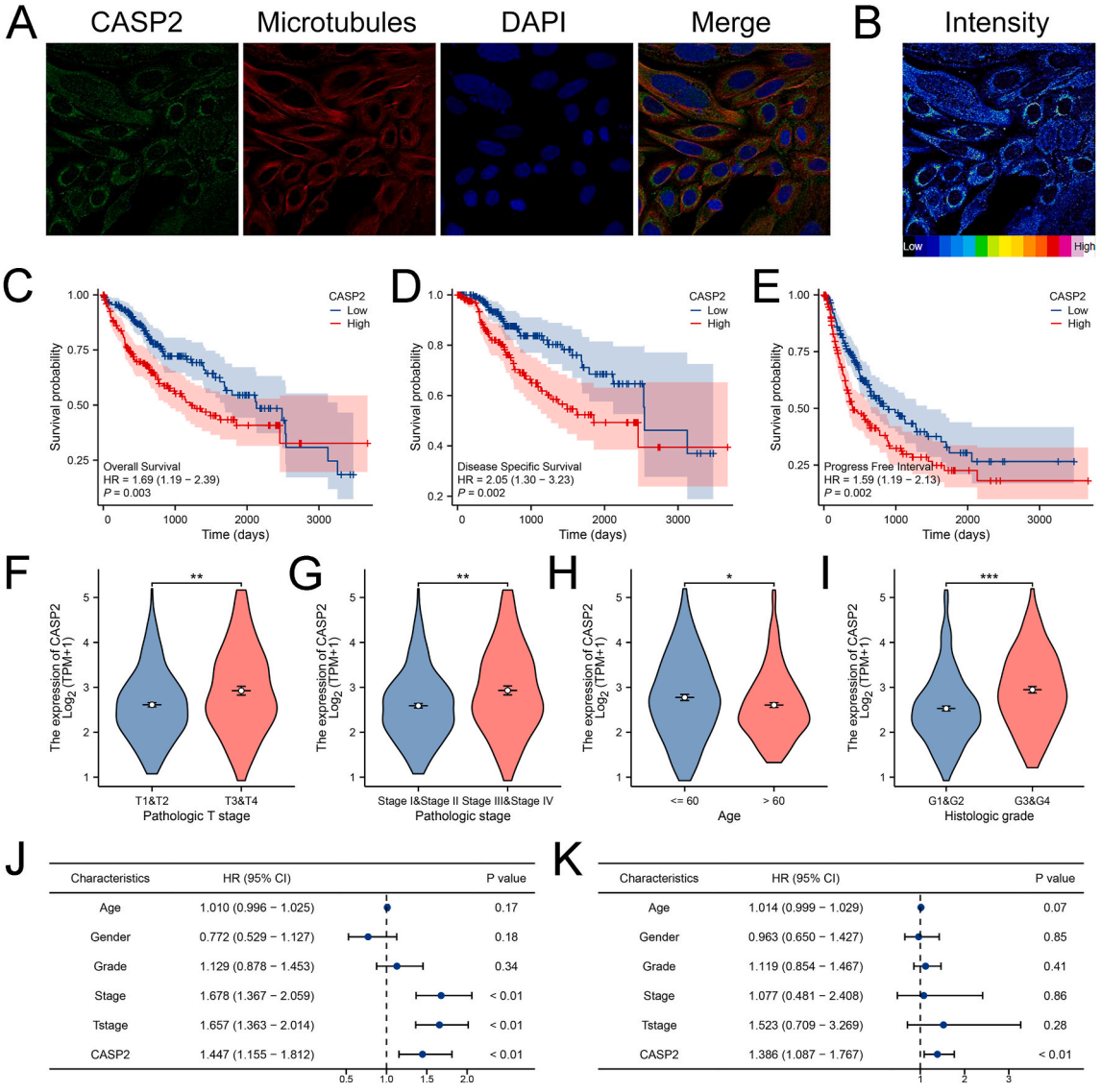

Fig. 2. Clinical role and expression pattern of CASP2 in HCC. **Notes: A-B:** Subcellular localization of FADD of SiHa cells from the data obtained from HPA database; **C:** The OS difference of patients with high and low CASP2 expression; **D:** The difference in DSS among patients with high and low CASP2 expression; **E:** The difference in PFI among patients with high and low CASP2 expression; **F–I:** Clinical correlation of CASP2; **J-K:** Univariate and multivariate analysis of CASP2.

analysis. Moreover, we noticed that most of these prognosis-significant molecules were differentially expressed in HCC and normal tissue (Fig. 1D).

3.2. Expression pattern and clinical role of CASP2 in HCC

Subcellular localization results indicate that the CASP2 is mainly localized in the mitochondria (Fig. 2A–B; HPA database, SiHa). The KM survival curves indicated that individuals with elevated CASP2 levels exhibited unfavorable survival outcomes (Fig. 2C–E,

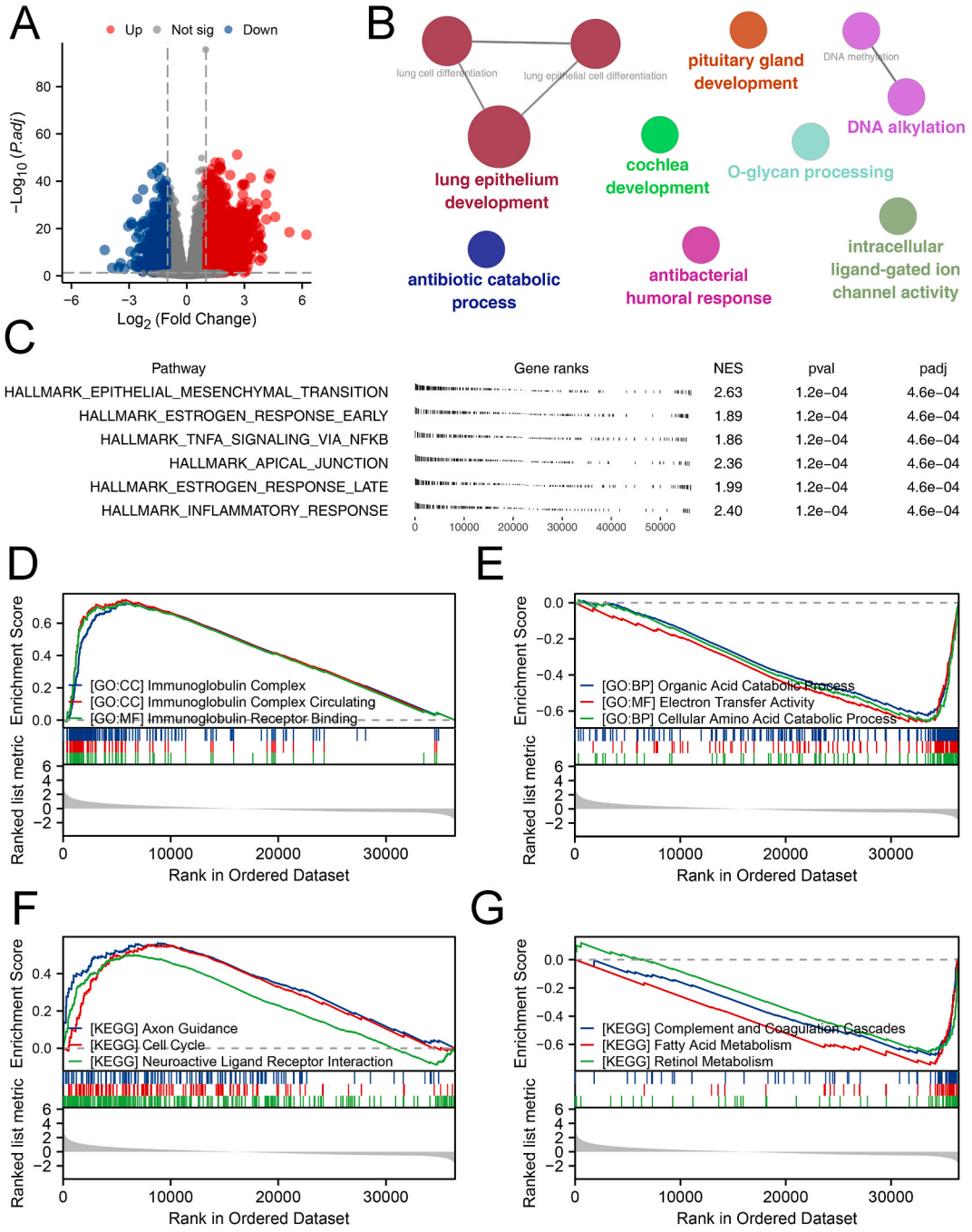

Fig. 3. Biological investigation of CASP2 in HCC microenvironment. **Notes: A:** DEGs analysis in patients with high and low CASP2 expression; **B:** ClueGO analysis of these DEGs; **C:** GSEA analysis of CASP2 based on Hallmark gene set; **D-E:** GSEA analysis based on GO gene set; **F-G:** GSEA analysis based on KEGG gene set.

overall survival, HR = 1.69, P = 0.003; disease-specific survival, HR = 2.05, P = 0.002; progression-free survival, HR = 1.59, P = 0.002). Meanwhile, we noticed that CASP2 is associated with worse clinical features (Fig. 2F–I, T3&4, stage III&IV, >60 years old and G3&4). Moreover, both univariate and multivariate analysis demonstrated that CASP2 serves as an autonomous prognostic indicator for HCC (Fig. 2J–K).

3.3. Biological enrichment analysis

To illustrate the biological role of CASP2 in HCC, an initial analysis was conducted on patients with varying levels of CASP2 expression to identify DEGs (Fig. 3A). ClueGO analysis indicated that CASP2 is mainly involved in lung epithelium development, cochlea development, pituitary gland development, DNA alkylation, O-glycan processing, antibiotic catabolic process, antibacterial humoral response and intracellular ligand-gated ion channel activity (Fig. 3B). GSEA analysis based on the Hallmark gene set showed epithelial-mesenchymal transition, estrogen response early, TNF-α signaling via NFKB, apical junction, late estrogen response and inflammatory response (Fig. 3C). Meanwhile, GSEA analysis based on GO terms indicated that the top three upregulated terms in

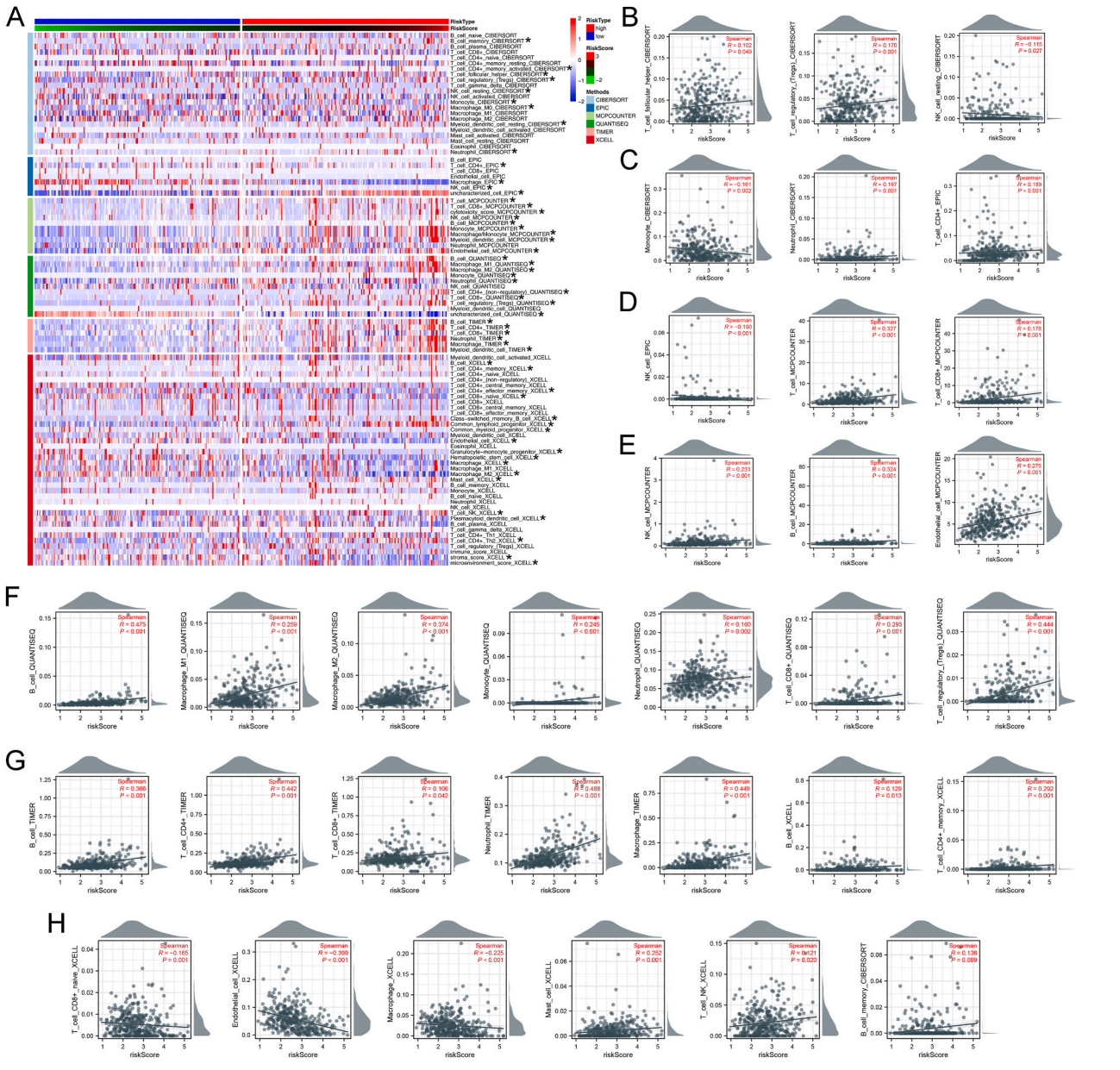

Fig. 4. Effect of CASP2 on immune infiltration and function. **Notes: A:** The correlation between quantified immune cells and CASP2; **B–H:** Correlation between CASP2 and specific immune cells.

patients with high CASP2 expression are immunoglobulin complex, immunoglobulin complex circulating and immunoglobulin receptor binding (Fig. 3D), yet the top three downregulated terms were organic acid catabolic process, electron transfer activity and cellular amino acid catabolic process (Fig. 3E). Moreover. GSEA analysis based on KEGG terms showed that the top three upregulated terms in patients with high CASP2 expression are axon guidance, cell cycle and neuroactive ligand-receptor interaction (Fig. 3F), yet the top three downregulated terms were complement and coagulation cascades, fatty acid metabolism and retinol metabolism (Fig. 3G).

3.4. Immune microenvironment analysis

Tumor progression is significantly influenced by the immune microenvironment. Consequently, we explored the effect of CASP2 on HCC microenvironment. The findings suggested that individuals exhibiting elevated CASP2 expression are more likely to experience increased levels of M2 macrophage, monocyte, endothelial cell, B cell, $CD4^+$ T cell, and common lymphoid progenitor (Fig. 4A–H).

3.5. Immunotherapy, genomic features and drug sensitivity analysis

To improve the prognostic prediction ability of CASP2, we developed a nomogram by combining CASP2 expression and clinical parameters (Fig. 5A). Moreover, the calibration graphs demonstrated that the projected survival from the nomogram plot aligns well with the observed survival (Fig. 5B). Immunotherapy is an emerging therapy for liver cancer. Hence, we aimed to investigate the impact of CASP2 on the responsiveness of liver cancer to immunotherapy. Notably, it was found that the majority of immune checkpoints exhibited distinct expression patterns in individuals with varying levels of CASP2 expression (Fig. 5C). Moreover, there

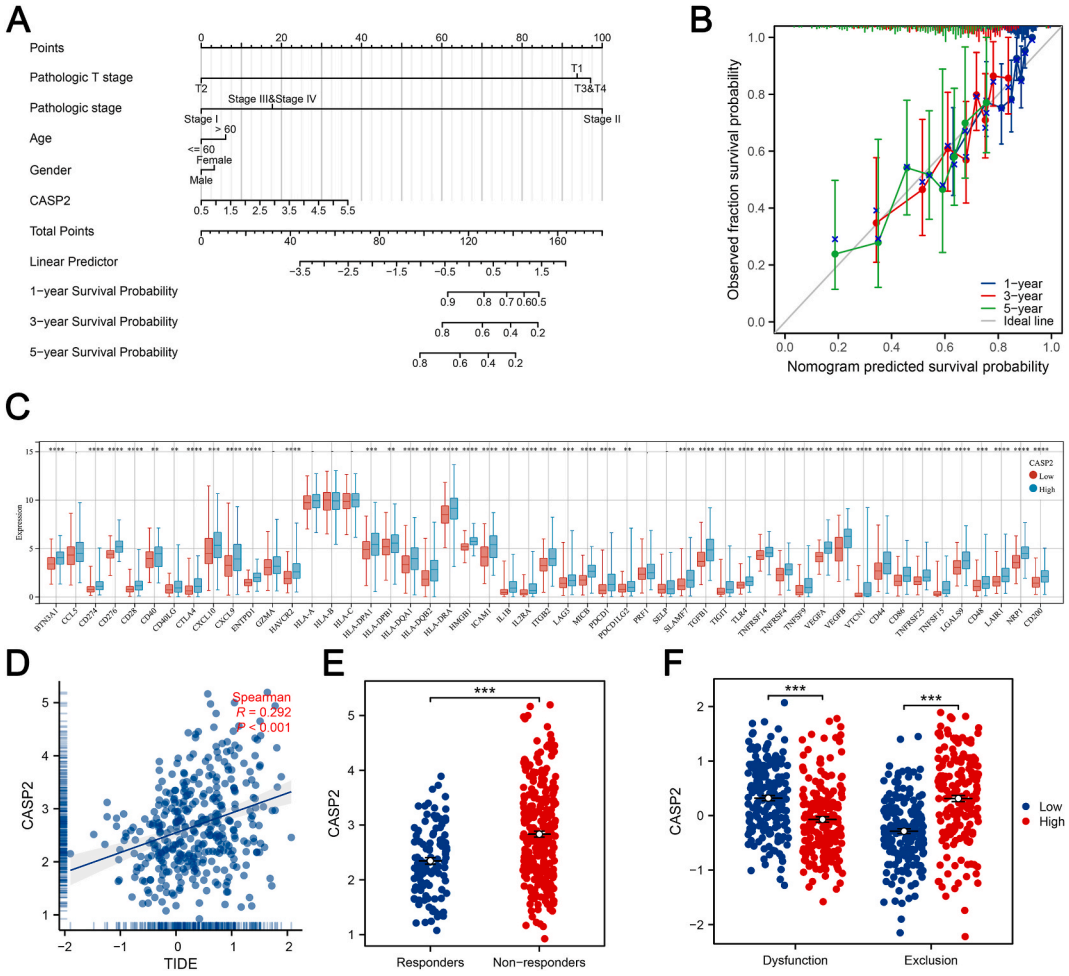

Fig. 5. Nomogram plot and immunotherapy response of CASP2. **Notes: A:** A nomogram plot was constructed based on clinical features and CASP2; **B:** Calibration curves of the nomogram plot; **C:** The level of immune checkpoint points molecules in patients with high and low CASP2 expression; **D:** Correlation between TIDE score and CASP2; **E:** The expression level of CASP2 in immunotherapy responders and non-responders; **F:** The immune dysfunction and exclusion in patients with high and low CASP2 expression.

was a significant association observed between the expression of CASP2 and TIDE score (Fig. 5D, R = 0.292, P < 0.001). In the meantime, it was observed that the individuals who did not respond to immunotherapy exhibited an increased expression of CASP2 (Fig. 5E). To be noted, the patients with high immune dysfunction status have lower CASP2 expression, but the immune exclusion was contrary (Fig. 5F). Next, we illustrated the overall mutation state of HCC based on the data from the TCGA database (Fig. 6A). Fig. 6B demonstrated that individuals exhibiting elevated CASP2 expression have a higher susceptibility to TP53 mutations. Furthermore, the analysis of drug sensitivity suggested that individuals exhibiting elevated CASP2 levels could potentially have a heightened response to doxorubicin and vorinostat. However, they may display resistance towards erlotinib, lapatinib, sunitinib and temsirolimus (Fig. 6C).

3.6. Single-cell analysis of CASP2 and prognosis model derived from CASP2-related genes

Next, we investigated the cellular expression level of CASP2 at the individual cell level. The results indicated that CASP2 was distributed in various cells (Fig. 7A–F, GSE98638, GSE125449, GSE140228, GSE166635, GSE146115, GSE146409 cohorts). To maximize the clinical utility of CASP2, we additionally developed a prognostic model utilizing genes associated with CASP2. The top 100 molecules with positive or negative correlation with CASP2 are shown in Fig. 8A and B, respectively. Afterward, a univariate Cox regression analysis was conducted to determine the molecules that showed a significant correlation with the survival of patients (Fig. 8C). LASSO regression analysis is used for data dimensionality reduction (Fig. 8D–E). In the end, the construction of the prognosis model involved three molecules, namely TAF3, EZH2, and FTCD, as identified by multivariate Cox regression analysis (Fig. 8F). The risk score was computed using the equation "Risk score = TAF3 * 0.373 + EZH2 * 0.230 + FTCD * −0.105". ROC survival curves

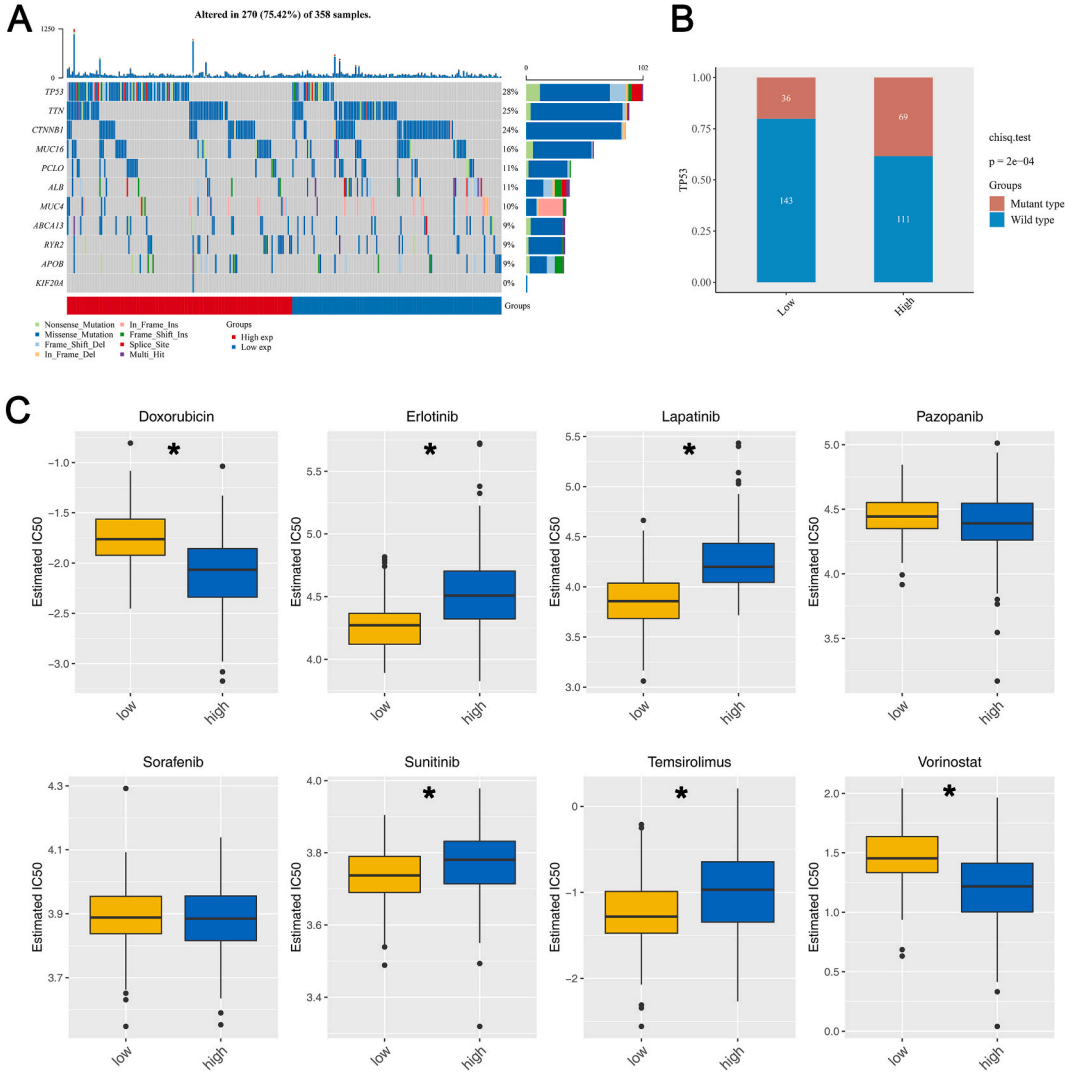

Fig. 6. Genomic instability and drug sensitivity of CASP2. **Notes: A:** Overview of the genomic feature of HCC; **B:** The mutation frequency of TP53 in patients with high and low CASP2 expression; **C:** The difference in drug sensitivity among patients with high and low CASP2 expression.

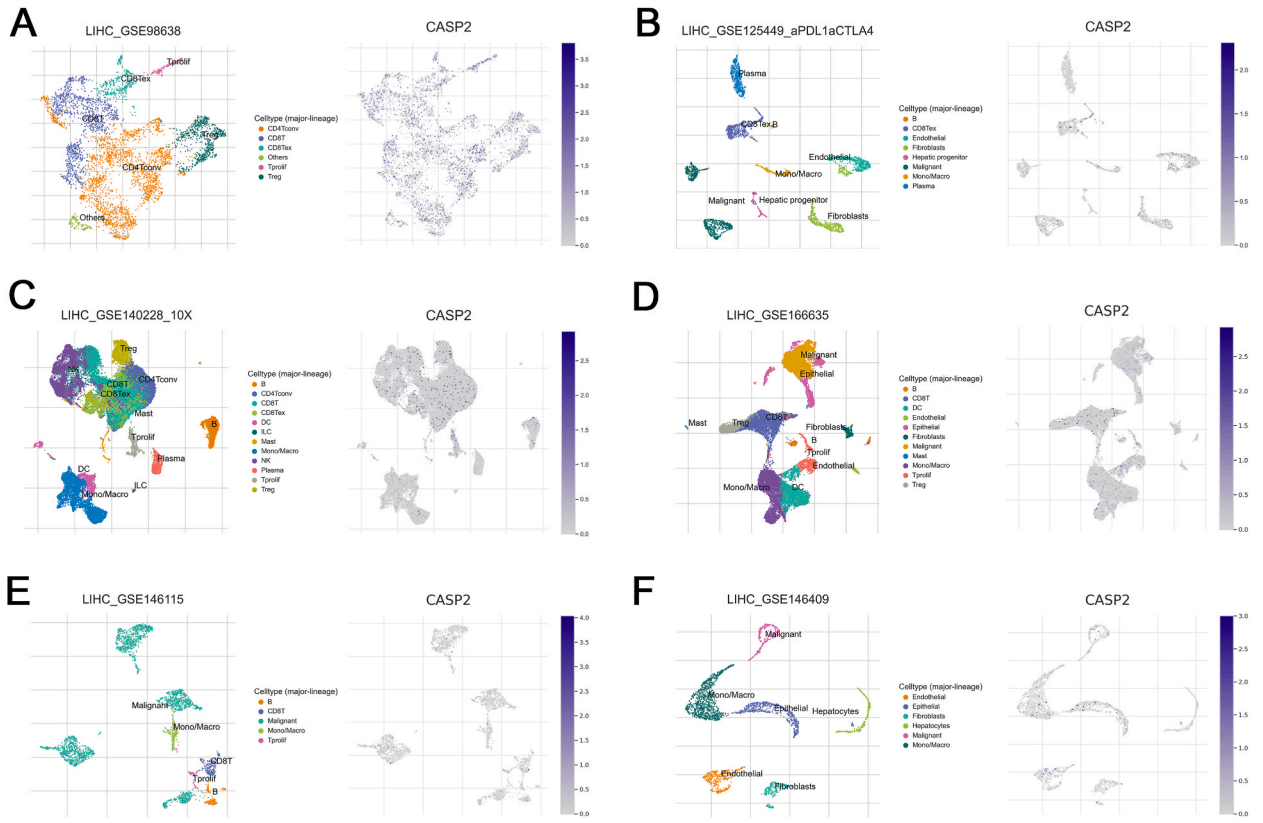

Fig. 7. Expression level of CASP2 at single cell level. **Notes: A:** Single-cell expression pattern of CASP2 in the GSE98638 cohort; **B:** Single-cell expression pattern of CASP2 in the GSE125449 cohort; C: Single-cell expression pattern of CASP2 in the GSE140228 cohort; **D:** Single-cell expression pattern of CASP2 in the GSE166635 cohort; **E:** Single-cell expression pattern of CASP2 in the GSE146115 cohort; **F:** Single-cell expression pattern of CASP2 in the GSE146409 cohort.

showed the good prognosis prediction efficiency of our model in the training cohort (Fig. 9A–C, TCGA cohort, 1-year AUC = 0.741, 3-year AUC = 0.698, 5-year AUC = 0.681). According to Fig. 9D, the KM survival curves indicated that individuals with elevated CASP2 levels could potentially experience a more unfavorable prognosis. Furthermore, we combined the ICGC data as the validation cohort using the Sva package (Fig. 9E–F). Moreover, our model also performed well in the validation cohort (Fig. 9G–J).

3.7. Knockdown of CASP2 remarkably promotes the proliferation, invasion and migration ability of HCC cells

Then, we tried to explore the effect of CASP2 on the biological behavior of HCC cells. Results of qRT-PCR showed that CASP2 is overexpressed in the HCC cells compared with the normal cells (Fig. 10A). Next, we knocked down the CASP2 for further experiments. The siRNA#2 has the best knockdown efficiency and is therefore selected for the next steps (Fig. 10B). CCK-8 and EdU assays showed that the inhibition of CASP2 can significantly promotes the cell proliferation ability of HCC cells (Fig. 10C–F). Transwell assay indicated that the knockdown of CASP2 can remarkably enhance the invasion and migration ability of HCC cells (Fig. 10G–I).

4. Discussion

In our study, we comprehensively explored the role of PANoptosis-related genes in HCC. The CASP2 was identified as the interest gene for further analysis. We found that CASP2 is related to the poor prognosis and worse clinical features of HCC patients. Moreover, we explored the biological pathway CASP2 is involved in and found that CASP2 is associated with multiple carcinogenic pathways. Also, we noticed that CASP2 can significantly reshape the HCC immune microenvironment and affect the response rate of immunotherapy. Analysis of drug sensitivity suggested that individuals exhibiting elevated CASP2 levels may display increased susceptibility to doxorubicin and vorinostat, while demonstrating resistance towards erlotinib, lapatinib, sunitinib, and temsirolimus. Meanwhile, we explored the single-cell distribution of CASP2 in the HCC microenvironment. To enhance the clinical application of CASP2 in HCC, we constructed a prognosis model using the molecules derived from CASP2, which demonstrated good efficiency in predicting patients prognosis. Moreover, in vitro experiments indicated that CASP2 can significantly inhibits cell proliferation, invasion and migration ability of HCC cells.

CASP2 is a key player in the regulation of cell death and is one of the earliest discovered members of the caspase family [38]. In

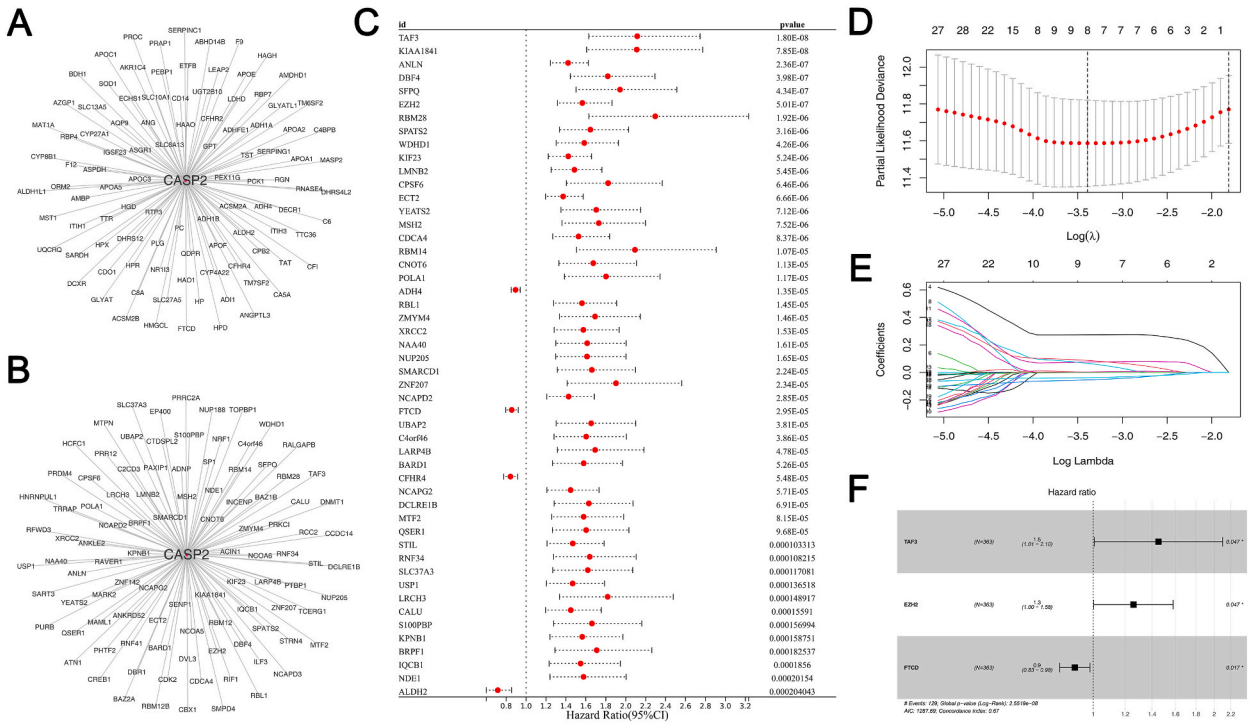

Fig. 8. Identification of the prognosis signature based on the CASP2-regulated genes. **Notes: A:** The top 100 molecules positively correlated with CASP2; **B:** The top 100 molecules negatively correlated with CASP2; **C:** Univariate Cox regression based on the CASP2-regulated genes; **D-E:** LASSO regression; **F:** Multivariate Cox regression based on the genes identified by LASSO regression.

diverse diseases, particularly cancer, the role of CASP2 is complex and multifaceted. CASP2 can function as a tumor suppressor by inducing apoptosis in response to genotoxic stress and preventing genomic instability, a key factor in tumorigenesis [39]. However, some studies suggest that CASP2 may also contribute to chemotherapy resistance in certain cancer types, demonstrating its potential dual role in cancer progression [40]. Huang et al. discovered that lncRNA TPT1-AS1 enhances the sensitivity of breast cancer cells to paclitaxel and suppresses cell growth through the miR-3156–5p/CASP2 pathway [41]. Chen et al. observed that Zingiberene can hinder the advancement of colon cancer by suppressing the PI3K/AKT/mTOR pathway and causing the deactivation of CASP2 [42]. While its function in cancer biology is not fully understood, the involvement of CASP2 in regulating cell death and its potential link to cancer makes it a significant area of interest in the ongoing search for effective cancer therapies.

Our results indicated that CAPS2 can regulate EMT signaling in the HCC based on the biological enrichment analysis. EMT is a biological phenomenon where epithelial cells acquire a mesenchymal phenotype, resulting in enhanced cell motility and invasiveness [43]. In the context of cancer, EMT plays a critical role in tumor progression, particularly in the metastasis process [44]. EMT enables the separation of cancer cells from the main tumor, infiltration into neighboring tissues, and dissemination to remote locations, ultimately promoting the metastasis of cancer throughout the body [45]. Additionally, EMT is implicated in therapeutic resistance, as cells undergoing EMT often exhibit increased resistance to chemotherapy and radiation therapy [46]. However, the precise mechanisms and regulatory pathways of EMT in cancer are still under active investigation.

Meanwhile, we found that CASP2 can affect the immune microenvironment of HCC. The results indicated that the patients with high CASP2 expression tend to have a higher infiltration level of M2 macrophage, monocyte, endothelial cell, B cell, $CD4^+$ T cell, and common lymphoid progenitor. Monocytes and macrophages are critical components of the immune system and play diverse roles in various diseases, including cancer [47,48]. Monocytes can differentiate into a variety of cell types, including M2 macrophages, depending on the tissue environment and specific signals. M2 macrophages, often referred to as “tumor-associated macrophages,” are known to play a significant role in cancer progression [49]. Unlike their M1 counterparts, which have anti-tumor properties, M2 macrophages promote tumor growth, invasiveness, and metastasis by secreting growth factors and anti-inflammatory cytokines [50]. They also contribute to angiogenesis, immune suppression, and therapeutic resistance. Monocytes in the tumor microenvironment can be recruited and polarized into M2 macrophages, thereby supporting tumor growth and progression. Therefore, strategies targeting the monocyte-M2 macrophage axis represent a promising area of cancer therapy research.

This study is not without limitations. Firstly, while bioinformatics data analysis has been an invaluable tool in exploring biological mechanisms and patterns, it is important to acknowledge that computational predictions might not fully represent the complex biological reality. Experimental validation is required to confirm our bioinformatically derived findings. Secondly, our study is primarily based on patient data from Western populations. Given the known genetic and lifestyle differences among different ethnic groups, our findings may not be fully generalizable to non-Western populations. Thus, the results should be interpreted with caution

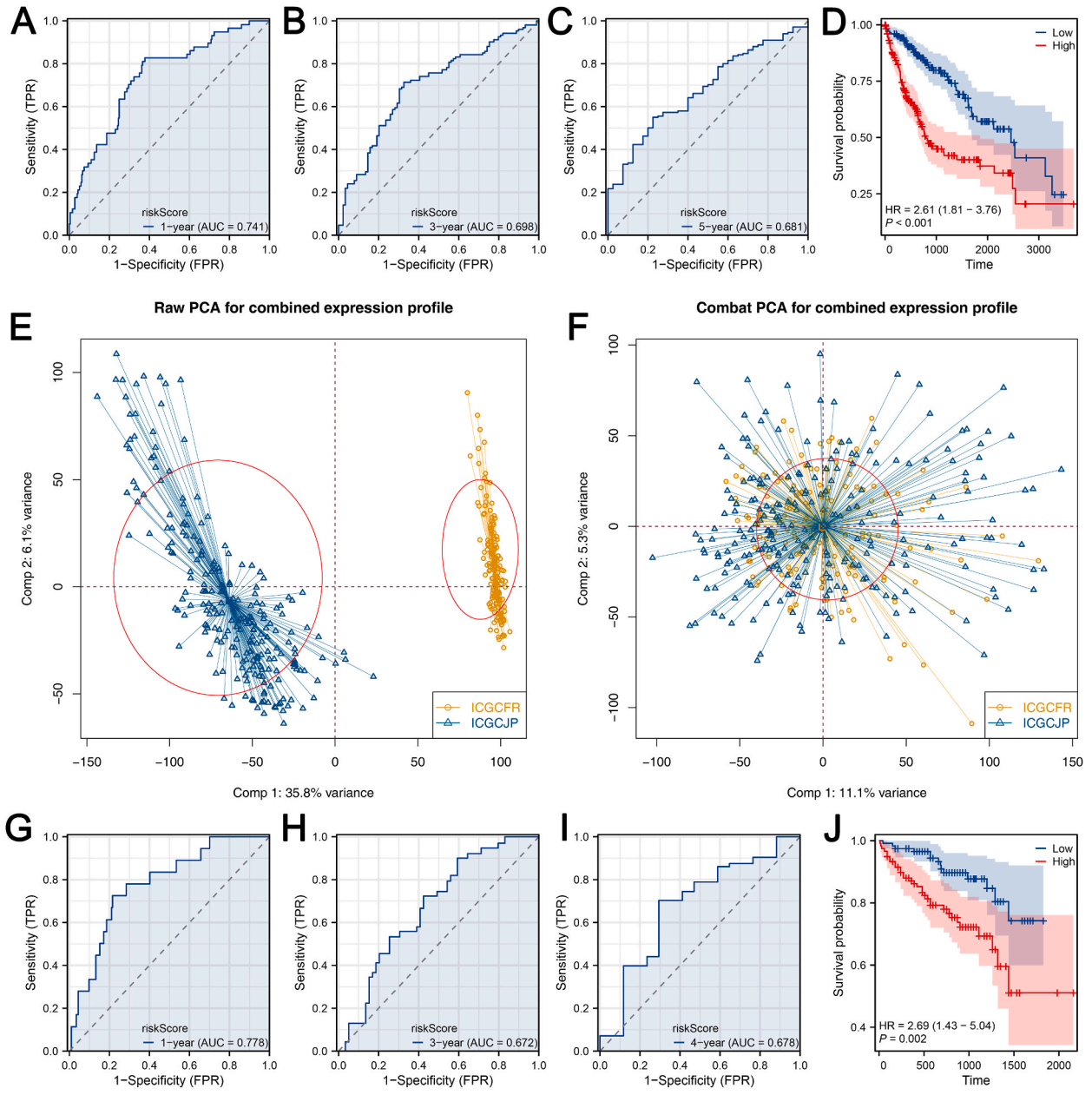

Fig. 9. Assessment of the prognosis signature in HCC. **Notes: A-D:** The performance of our signature in the training cohort; **E-F:** Two ICGC cohorts were combined as the validation cohorts; **G-J:** The performance of our signature in the external validation cohort.

when applied to diverse ethnic groups, and further studies involving different ethnicities are needed to validate and expand our findings. Lastly, the lack of complete clinical data for some patients may affect the robustness of our conclusions. Missing data could potentially introduce bias and limit the statistical power of the study, thereby affecting the reliability and validity of our results. Future studies with more comprehensive and complete datasets will be required to confirm our findings and further understand the complex mechanisms at play.

Funding

None.

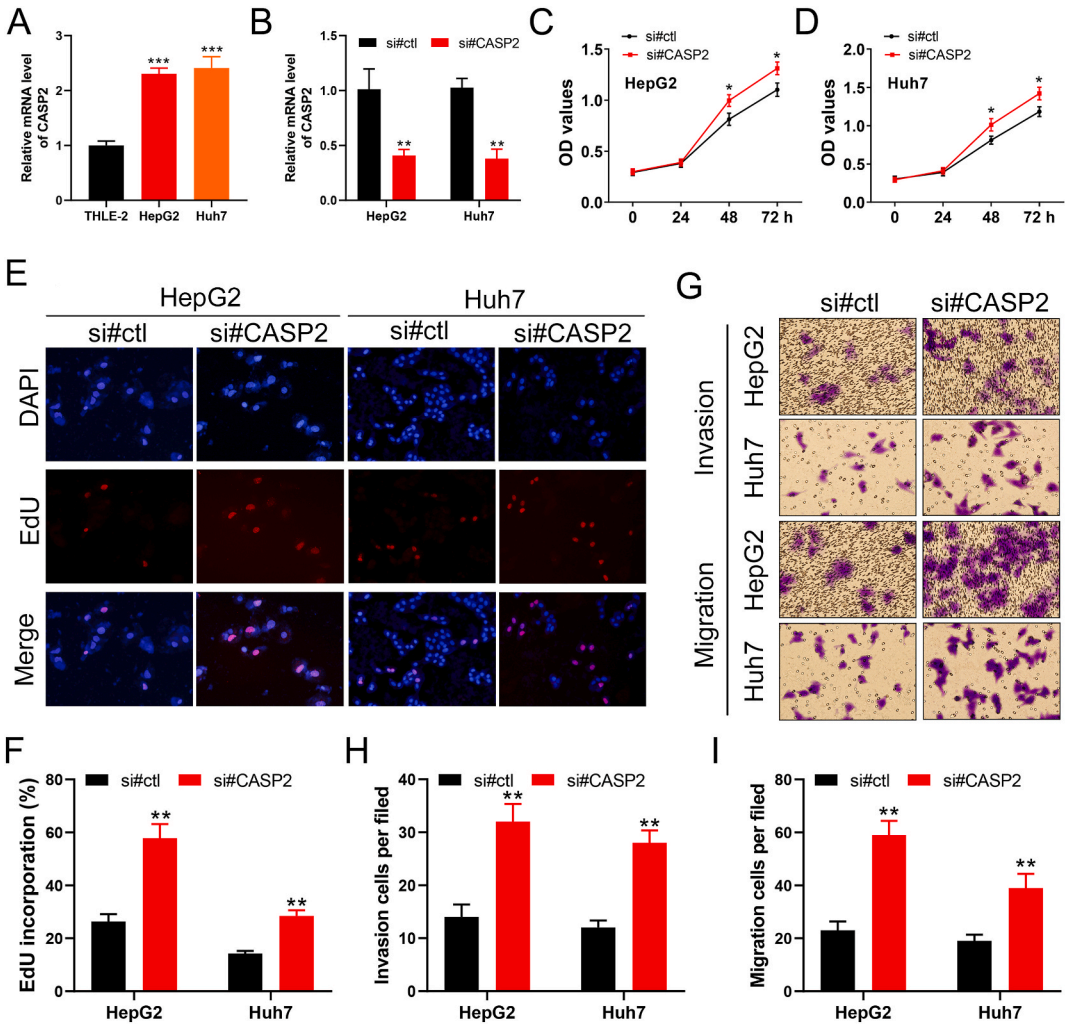

Fig. 10. The knockdown of CASP2 significantly promotes the proliferation, invasion and migration ability of HCC cells. **Notes: A:** The expression level of CASP2 in normal and HCC cells; **B:** qRT-PCR was used to evaluate the knockdown efficiency of CASP2 in HepG2 and Huh7 cells; **C-D:** CCK-8 assay was performed in the control and CASP2 knockdown cells; **E-F:** EdU assay was performed in the control and CASP2 knockdown cells; **G-I:** Transwell assay was performed in the control and CASP2 knockdown cells.

Data availability statement

Data will be made available on request.

CRediT authorship contribution statement

Yichao Lou: Writing – review & editing, Writing – original draft, Visualization, Validation, Supervision, Software, Resources, Project administration, Methodology, Investigation, Funding acquisition, Formal analysis, Data curation, Conceptualization. **Desheng Chen:** Formal analysis, Data curation, Conceptualization. **Qi Gu:** Visualization, Validation, Supervision, Software. **Qi Zhu:** Software, Resources, Project administration, Conceptualization. **Hongcheng Sun:** Writing – review & editing, Writing – original draft, Visualization, Validation, Supervision, Software, Resources, Project administration, Methodology, Investigation, Funding acquisition, Formal analysis, Data curation, Conceptualization.

Declaration of competing interest

The authors declare that they have no known competing financial interests or personal relationships that could have appeared to influence the work reported in this paper.

Acknowledgment

None.

Appendix A. Supplementary data

Supplementary data to this article can be found online at https://doi.org/10.1016/j.heliyon.2024.e27302.

References

[1] L. Li, H. Wang, Heterogeneity of liver cancer and personalized therapy, Cancer Lett. 379 (2) (2016 Sep 1) 191–197. PubMed PMID: 26213370. Epub 2015/07/28. eng.
[2] J. Bruix, K.H. Han, G. Gores, J.M. Llovet, V. Mazzaferro, Liver cancer: approaching a personalized care, J. Hepatol. 62 (1 Suppl) (2015 Apr) S144–S156. PubMed PMID: 25920083. Pubmed Central PMCID: PMC4520430. Epub 2015/04/29. eng.
[3] J.M. Llovet, R.K. Kelley, A. Villanueva, A.G. Singal, E. Pikarsky, S. Roayaie, et al., Hepatocellular carcinoma, Nat. Rev. Dis. Prim. 7 (1) (2021 Jan 21) 6. PubMed PMID: 33479224. Epub 2021/01/23. eng.
[4] H. Ochi, A. Hiraoka, M. Hirooka, Y. Koizumi, M. Amano, N. Azemoto, et al., Direct-acting antivirals improve survival and recurrence rates after treatment of hepatocellular carcinoma within the Milan criteria, J. Gastroenterol. 56 (1) (2021 Jan) 90–100. PubMed PMID: 33278003. Pubmed Central PMCID: PMC7819935. Epub 2020/12/06. eng.
[5] Y. Zhao, Y.N. Zhang, K.T. Wang, L. Chen, Lenvatinib for hepatocellular carcinoma: from preclinical mechanisms to anti-cancer therapy, Biochim. Biophys. Acta Rev. Canc 1874 (1) (2020 Aug) 188391. PubMed PMID: 32659252. Epub 2020/07/14. eng.
[6] T. Couri, A. Pillai, Goals and targets for personalized therapy for HCC, Hepatology international 13 (2) (2019 Mar) 125–137. PubMed PMID: 30600478. Epub 2019/01/03. eng.
[7] M. Zheng, T.D. Kanneganti, The regulation of the ZBP1-NLRP3 inflammasome and its implications in pyroptosis, apoptosis, and necroptosis (PANoptosis), Immunol. Rev. 297 (1) (2020 Sep) 26–38. PubMed PMID: 32729116. Pubmed Central PMCID: PMC7811275. Epub 2020/07/31. eng.
[8] R. Karki, B. Sundaram, B.R. Sharma, S. Lee, R.K.S. Malireddi, L.N. Nguyen, et al., ADAR1 restricts ZBP1-mediated immune response and PANoptosis to promote tumorigenesis, Cell Rep. 37 (3) (2021 Oct 19) 109858. PubMed PMID: 34686350. Pubmed Central PMCID: PMC8853634. Epub 2021/10/24. eng.
[9] R. Karki, S. Lee, R. Mall, N. Pandian, Y. Wang, B.R. Sharma, et al., ZBP1-dependent inflammatory cell death, PANoptosis, and cytokine storm disrupt IFN therapeutic efficacy during coronavirus infection, Science immunology 7 (74) (2022 Aug 26) eabo6294. PubMed PMID: 35587515. Pubmed Central PMCID: PMC9161373. Epub 2022/05/20. eng.
[10] J.F. Lin, P.S. Hu, Y.Y. Wang, Y.T. Tan, K. Yu, K. Liao, et al., Phosphorylated NFS1 weakens oxaliplatin-based chemosensitivity of colorectal cancer by preventing PANoptosis. Signal transduction and targeted therapy, PubMed PMID: 35221331. Pubmed Central PMCID: PMC8882671. Epub 2022/03/01. eng 7 (1) (2022 Feb 28) 54.
[11] P. Zhu, Z.R. Ke, J.X. Chen, S.J. Li, T.L. Ma, X.L. Fan, Advances in mechanism and regulation of PANoptosis: prospects in disease treatment, Front. Immunol. 14 (2023) 1120034. PubMed PMID: 36845112. Pubmed Central PMCID: PMC9948402. Epub 2023/02/28. eng.
[12] J. Liu, M. Hong, Y. Li, D. Chen, Y. Wu, Y. Hu, Programmed cell death tunes tumor immunity, Front. Immunol. 13 (2022) 847345. PubMed PMID: 35432318. Pubmed Central PMCID: PMC9005769. Epub 2022/04/19. eng.
[13] J.M. Gullett, R.E. Tweedell, T.D. Kanneganti, It's all in the PAN: crosstalk, plasticity, redundancies, switches, and interconnectedness encompassed by PANoptosis underlying the totality of cell death-associated biological effects, Cells 11 (9) (2022 Apr 29). PubMed PMID: 35563804. Pubmed Central PMCID: PMC9105755. Epub 2022/05/15. eng.
[14] X. Shi, X. Gao, W. Liu, X. Tang, J. Liu, D. Pan, et al., Construction of the panoptosis-related gene model and characterization of tumor microenvironment infiltration in hepatocellular carcinoma, Oncology research 31 (4) (2023) 569–590. PubMed PMID: 37415742. Pubmed Central PMCID: PMC10319585. Epub 2023/07/07. eng.
[15] Z. Wang, M.A. Jensen, J.C. Zenklusen, A practical guide to the cancer genome atlas (TCGA), Methods Mol. Biol. 1418 (2016) 111–141. PubMed PMID: 27008012. Epub 2016/03/24. eng.
[16] S. Wei, Z. Chen, X. Ling, W. Zhang, L. Jiang, Comprehensive analysis illustrating the role of PANoptosis-related genes in lung cancer based on bioinformatic algorithms and experiments, Front. Pharmacol. 14 (2023) 1115221. PubMed PMID: 36874021. Pubmed Central PMCID: PMC9977813. Epub 2023/03/07. eng.
[17] P.J. Thul, L. Åkesson, M. Wiking, D. Mahdessian, A. Geladaki, H. Ait Blal, et al., A subcellular map of the human proteome, Science (New York, NY) 356 (6340) (2017 May 26). PubMed PMID: 28495876. Epub 2017/05/13. eng.
[18] J.T. Leek, W.E. Johnson, H.S. Parker, A.E. Jaffe, J.D. Storey, The sva package for removing batch effects and other unwanted variation in high-throughput experiments, Bioinformatics 28 (6) (2012 Mar 15) 882–883. PubMed PMID: 22257669. Pubmed Central PMCID: PMC3307112. Epub 2012/01/20. eng.
[19] A. Subramanian, P. Tamayo, V.K. Mootha, S. Mukherjee, B.L. Ebert, M.A. Gillette, et al., Gene set enrichment analysis: a knowledge-based approach for interpreting genome-wide expression profiles, Proc. Natl. Acad. Sci. U.S.A. 102 (43) (2005 Oct 25) 15545–15550. PubMed PMID: 16199517. Pubmed Central PMCID: PMC1239896. Epub 2005/10/04. eng.
[20] G. Bindea, B. Mlecnik, H. Hackl, P. Charoentong, M. Tosolini, A. Kirilovsky, et al., ClueGO: a Cytoscape plug-in to decipher functionally grouped gene ontology and pathway annotation networks, Bioinformatics 25 (8) (2009 Apr 15) 1091–1093. PubMed PMID: 19237447. Pubmed Central PMCID: PMC2666812. Epub 2009/02/25. eng.
[21] B. Chen, M.S. Khodadoust, C.L. Liu, A.M. Newman, A.A. Alizadeh, Profiling tumor infiltrating immune cells with CIBERSORT, Methods Mol. Biol. 1711 (2018) 243–259. PubMed PMID: 29344893. Pubmed Central PMCID: PMC5895181. Epub 2018/01/19. eng.
[22] J. Racle, D. Gfeller, EPIC: a tool to estimate the proportions of different cell types from bulk gene expression data, Methods Mol. Biol. 2120 (2020) 233–248. PubMed PMID: 32124324. Epub 2020/03/04. eng.
[23] E. Becht, N.A. Giraldo, L. Lacroix, B. Buttard, N. Elarouci, F. Petitprez, et al., Estimating the population abundance of tissue-infiltrating immune and stromal cell populations using gene expression, Genome Biol. 17 (1) (2016 Oct 20) 218. PubMed PMID: 27765066. Pubmed Central PMCID: PMC5073889. Epub 2016/10/22. eng.
[24] C. Plattner, F. Finotello, D. Rieder, Deconvoluting tumor-infiltrating immune cells from RNA-seq data using quanTIseq, Methods Enzymol. 636 (2020) 261–285. PubMed PMID: 32178821. Epub 2020/03/18. eng.
[25] T. Li, J. Fan, B. Wang, N. Traugh, Q. Chen, J.S. Liu, et al., TIMER: a web server for comprehensive analysis of tumor-infiltrating immune cells, Cancer Res. 77 (21) (2017 Nov 1) e108–e110. PubMed PMID: 29092952. Pubmed Central PMCID: PMC6042652. Epub 2017/11/03. eng.
[26] D. Aran, Z. Hu, A.J. Butte, xCell: digitally portraying the tissue cellular heterogeneity landscape, Genome Biol. 18 (1) (2017 Nov 15) 220. PubMed PMID: 29141660. Pubmed Central PMCID: PMC5688663 The authors declare that they have no competing interests. PUBLISHER'S NOTE: Springer Nature remains neutral with regard to jurisdictional claims in published maps and institutional affiliations. Epub 2017/11/17. eng.
[27] S. Hänzelmann, R. Castelo, J. Guinney, GSVA: gene set variation analysis for microarray and RNA-seq data, BMC Bioinf. 14 (7) (2013 Jan 16). PubMed PMID: 23323831. Pubmed Central PMCID: PMC3618321. Epub 2013/01/18. eng.

[28] J. Fu, K. Li, W. Zhang, C. Wan, J. Zhang, P. Jiang, et al., Large-scale public data reuse to model immunotherapy response and resistance, Genome Med. 12 (1) (2020 Feb 26) 21. PubMed PMID: 32102694. Pubmed Central PMCID: PMC7045518. Epub 2020/02/28. eng.
[29] W. Yang, J. Soares, P. Greninger, E.J. Edelman, H. Lightfoot, S. Forbes, et al., Genomics of Drug Sensitivity in Cancer (GDSC): a resource for therapeutic biomarker discovery in cancer cells (Database issue), Nucleic Acids Res. 41 (2013 Jan) D955–D961. PubMed PMID: 23180760. Pubmed Central PMCID: PMC3531057. Epub 2012/11/28. eng.
[30] D. Sun, J. Wang, Y. Han, X. Dong, J. Ge, R. Zheng, et al., TISCH: a comprehensive web resource enabling interactive single-cell transcriptome visualization of tumor microenvironment, D1420-d30, Nucleic Acids Res. 49 (D1) (2021 Jan 8). PubMed PMID: 33179754. Pubmed Central PMCID: PMC7778907. Epub 2020/11/13. eng.
[31] C. Zheng, L. Zheng, J.K. Yoo, H. Guo, Y. Zhang, X. Guo, et al., Landscape of infiltrating T cells in liver cancer revealed by single-cell sequencing, Cell 169 (7) (2017 Jun 15) 1342–1356, e16. PubMed PMID: 28622514. Epub 2017/06/18. eng.
[32] L. Ma, M.O. Hernandez, Y. Zhao, M. Mehta, B. Tran, M. Kelly, et al., Tumor cell biodiversity drives microenvironmental reprogramming in liver cancer, Cancer Cell 36 (4) (2019 Oct 14) 418–430, e6. PubMed PMID: 31588021. Pubmed Central PMCID: PMC6801104. Epub 2019/10/08. eng.
[33] Q. Zhang, Y. He, N. Luo, S.J. Patel, Y. Han, R. Gao, et al., Landscape and dynamics of single immune cells in hepatocellular carcinoma, Cell 179 (4) (2019 Oct 31) 829–845, e20. PubMed PMID: 31675496. Epub 2019/11/02. eng.
[34] Y. Meng, Q. Zhao, L. An, S. Jiao, R. Li, Y. Sang, et al., A TNFR2-hnRNPK Axis promotes primary liver cancer development via activation of YAP signaling in hepatic progenitor cells, Cancer Res. 81 (11) (2021 Jun 1) 3036–3050. PubMed PMID: 33619115. Epub 2021/02/24. eng.
[35] X. Su, L. Zhao, Y. Shi, R. Zhang, Q. Long, S. Bai, et al., Clonal evolution in liver cancer at single-cell and single-variant resolution, J. Hematol. Oncol. 14 (1) (2021 Feb 2) 22. PubMed PMID: 33531041. Pubmed Central PMCID: PMC7852352. Epub 2021/02/04. eng.
[36] H. Massalha, K. Bahar Halpern, S. Abu-Gazala, T. Jana, E.E. Massasa, A.E. Moor, et al., A single cell atlas of the human liver tumor microenvironment, Mol. Syst. Biol. 16 (12) (2020 Dec) e9682. PubMed PMID: 33332768. Pubmed Central PMCID: PMC7746227. Epub 2020/12/18. eng.
[37] M.E. Ritchie, B. Phipson, D. Wu, Y. Hu, C.W. Law, W. Shi, et al., Limma powers differential expression analyses for RNA-sequencing and microarray studies, Nucleic Acids Res. 43 (7) (2015 Apr 20) e47. PubMed PMID: 25605792. Pubmed Central PMCID: PMC4402510. Epub 2015/01/22. eng.
[38] M. Tiwari, L.K. Sharma, D. Vanegas, D.A. Callaway, Y. Bai, J.D. Lechleiter, et al., A nonapoptotic role for CASP2/caspase 2: modulation of autophagy, Autophagy 10 (6) (2014 Jun) 1054–1070. PubMed PMID: 24879153. Pubmed Central PMCID: PMC4091168. Epub 2014/06/01. eng.
[39] G.S. Kopeina, B. Zhivotovsky, Caspase-2 as a master regulator of genomic stability, Trends Cell Biol. 31 (9) (2021 Sep) 712–720. PubMed PMID: 33752921. Epub 2021/03/24. eng.
[40] M. Ashrafizadeh, A. Zarrabi, K. Hushmandi, F. Hashemi, E.R. Moghadam, M. Owrang, et al., Lung cancer cells and their sensitivity/resistance to cisplatin chemotherapy: role of microRNAs and upstream mediators, Cell. Signal. 78 (2021 Feb) 109871. PubMed PMID: 33279671. Epub 2020/12/07. eng.
[41] Y. Huang, Y. Zheng, X. Shao, L. Shi, G. Li, P. Huang, Long non-coding RNA TPT1-AS1 sensitizes breast cancer cell to paclitaxel and inhibits cell proliferation by miR-3156-5p/caspase 2 axis, Hum. Cell 34 (4) (2021 Jul) 1244–1254. PubMed PMID: 33999360. Epub 2021/05/18. eng.
[42] H. Chen, X. Tang, T. Liu, L. Jing, J. Wu, Zingiberene inhibits in vitro and in vivo human colon cancer cell growth via autophagy induction, suppression of PI3K/AKT/mTOR Pathway and caspase 2 deactivation, Journal of BUON : official journal of the Balkan Union of Oncology 24 (4) (2019 Jul-Aug) 1470–1475. PubMed PMID: 31646793. Epub 2019/10/28. eng.
[43] R. Gundamaraju, W. Lu, M.K. Paul, N.K. Jha, P.K. Gupta, S. Ojha, et al., Autophagy and EMT in cancer and metastasis: who controls whom? Biochim. Biophys. Acta, Mol. Basis Dis. 1868 (9) (2022 Sep 1) 166431. PubMed PMID: 35533903. Epub 2022/05/10. eng.
[44] Y. Huang, W. Hong, X. Wei, The molecular mechanisms and therapeutic strategies of EMT in tumor progression and metastasis, J. Hematol. Oncol. 15 (1) (2022 Sep 8) 129. PubMed PMID: 36076302. Pubmed Central PMCID: PMC9461252. Epub 2022/09/09. eng.
[45] E. Sabouni, M.M. Nejad, S. Mojtabavi, S. Khoshduz, M. Mojtabavi, N. Nadafzadeh, et al., Unraveling the function of epithelial-mesenchymal transition (EMT) in colorectal cancer: metastasis, therapy response, and revisiting molecular pathways, Biomedicine & pharmacotherapy = Biomedecine & pharmacotherapie 160 (2023 Apr) 114395. PubMed PMID: 36804124. Epub 2023/02/22. eng.
[46] M. Singh, N. Yelle, C. Venugopal, S.K. Singh, EMT: mechanisms and therapeutic implications, Pharmacol. Ther. 182 (2018 Feb) 80–94. PubMed PMID: 28834698. Epub 2017/08/24. eng.
[47] C.E. Olingy, H.Q. Dinh, C.C. Hedrick, Monocyte heterogeneity and functions in cancer, J. Leukoc. Biol. 106 (2) (2019 Aug) 309–322. PubMed PMID: 30776148. Pubmed Central PMCID: PMC6658332. Epub 2019/02/19. eng.
[48] M. Genin, F. Clement, A. Fattaccioli, M. Raes, C. Michiels, M1 and M2 macrophages derived from THP-1 cells differentially modulate the response of cancer cells to etoposide, BMC Cancer 15 (2015 Aug 8) 577. PubMed PMID: 26253167. Pubmed Central PMCID: PMC4545815. Epub 2015/08/09. eng.
[49] Y. Chen, S. Zhang, Q. Wang, X. Zhang, Tumor-recruited M2 macrophages promote gastric and breast cancer metastasis via M2 macrophage-secreted CHI3L1 protein, J. Hematol. Oncol. 10 (1) (2017 Feb 1) 36. PubMed PMID: 28143526. Pubmed Central PMCID: PMC5286803. Epub 2017/02/02. eng.
[50] A. Shapouri-Moghaddam, S. Mohammadian, H. Vazini, M. Taghadosi, S.A. Esmaeili, F. Mardani, et al., Macrophage plasticity, polarization, and function in health and disease, J. Cell. Physiol. 233 (9) (2018 Sep) 6425–6440. PubMed PMID: 29319160. Epub 2018/01/11. eng.